$La_{0.95}Mg_{0.05}MnO_3$: an ideal ferromagnetic system?

2000 J. Phys.: Condens. Matter 12 6903

(http://iopscience.iop.org/0953-8984/12/30/318)

J. Phys.: Condens. Matter **12** (2000) 6903–6918. Printed in the UK PII: S0953-8984(00)13922-0

$La_{0.95}Mg_{0.05}MnO_3$: an ideal ferromagnetic system?

J H Zhao, T Song, H P Kunkel, X Z Zhou, R M Roshko and Gwyn Williams

Department of Physics and Astronomy, University of Manitoba, Winnipeg, MB, R3T 2N2, Canada

Received 16 May 2000

Abstract. Detailed measurements of the field- and temperature-dependent ac susceptibility and magnetization of $LaMnO_3$ substituted with 5 at.% of the divalent cation Mg are presented. This system is a semiconducting *ferromagnet* at low temperature; in particular, analysis of these data yields $T_c = 147.2 \pm 0.2$ K, with critical exponents $\delta = 4.75 \pm 0.15$ (from the field dependence of the susceptibility along the 'crossover' line, and confirmed by measurements along the critical isotherm), $\gamma + \beta = 1.75 \pm 0.05$ (from the temperature dependence of the crossover line) and $\gamma = 1.39 \pm 0.05$ (from the temperature dependence of the susceptibility along the same line). Within experimental uncertainty these exponent values agree with those predicted by the isotropic, three-dimensional Heisenberg model. Nevertheless this system exhibits some unusual characteristics, specifically in the temperature dependence of the (low-) field-cooled and zero-field-cooled magnetization. The latter have been modelled by a Preisach-based approach, which helps to resolve a ubiquitous dilemma in the doped manganites, *viz.* the appearance of a technical hardness irreconcilable with low coercive field values. A possible origin for the large, reversible component in the response below T_c is presented.

1. Introduction

While colossal magnetoresistance (CMR) has been an established property [1] of doped manganese perovskites since the 1950s, renewed interest in these and related systems has arisen recently as a result of both applied and fundamental considerations [2]. Of particular current interest in the first category is the ability to tune the doping to produce half-metallic ferromagnets, which raises the possibility of fabricating devices based on spin—rather than charge—transport, while in the second context these systems are regarded as examples of strongly correlated electronic materials, in the sense of strong *intra*-site rather than *inter*-site correlations, as estimated carrier densities lie in the range [3] 5×10^{-2}–5×10^{-1} fu^{-1}.

The doped manganese perovskites with general formula $L_{1-x}A_xMnO_3$ (L = rare earth or Y, A = divalent cation) correspond to the $n = \infty$ member of the Ruddlesden–Popper family of compounds [4] of general formula $(L, A)_{n+1}Mn_nO_{3n+1}$. Reducing n progressively decouples the perovskite layers, while for $n = \infty$ they are fully three dimensional, a point returned to below. While the role of divalent cations is well established—they result in an inhomogeneous distribution of mixed valent Mn^{3+}–Mn^{4+} ions to ensure charge neutrality—a full appreciation of their influence on both magnetic and transport properties is lacking currently. In terms of the transport properties, for doping levels, x, typically $\gtrsim 0.1$, the conjectured emergence of an $O(2p_\sigma)$–$Mn(e_g)$ 'band' enables the single e_g electron occupying the Mn^{3+} sites to acquire a degree of itineracy; however the strong intra-site correlations amongst the Mn 3d electrons (i.e. the strong Hund's rule coupling) favours Mn → O → Mn hopping (so-called double exchange) of such e_g electrons between neighbouring mixed valent sites only when

0953-8984/00/306903+16$30.00

the corresponding localized t_{2g} core spins are parallel. The latter leads to hopping/charge transfer integrals $t_{ij} \sim t_0 \cos(\theta_{ij}/2)$ between an interacting pair of neighbouring Mn atoms (labelled by sites i and j), where θ_{ij} is the angle between the corresponding core spins; the corresponding double exchange coupling between the spins S_i and S_j has the form $-J_0|\cos(\theta_{ij}/2)|S_iS_j$. Though such an approach yields a qualitative understanding of the increase in conductivity accompanying ferromagnetic ordering [5], and, through the field dependence of the ordering temperature, a basic understanding of CMR, it does not yield quantitative agreement. In essence, the scattering rate calculated within such an approach fails to yield the correct resistivity in the paramagnetic phase. This has led to suggestions of other processes being operative—particularly electron–lattice coupling processes, resulting not only in the possibility of polaronic transport in the paramagnetic phase [6] (along with the presence of both static/coherent and dynamic Jahn–Teller distortions, although these are still the subject of ongoing investigations [7]) but also in the ferromagnetic phase [8].

To date, perhaps the best studied system is $La_{1-x}Ca_xMnO_3$, for which a complete phase diagram is available [9]. Indeed the term 'optimal doping' was introduced to characterize this system, specifically the peak in the ferromagnetic ordering temperature T_c near $x \simeq 0.33$. Subsequently many other divalent cation substitutions near 'optimal doping' were effected, including relatively small cations such as Mg. The latter was [10]—along [11] with $CaCu_3Mn_4O_{12}$—amongst the first perovskite-like systems to be studied in which a ferromagnetic transition does not 'drive' a metal–insulator phase change. Here we report detailed measurements of the magnetic properties in the low-x region, specifically $x = 0.05$, which reveal that not only does this system respond as a ferromagnet, but in many respects it behaves as an ideal one. This system also retains semiconducting characteristics in the ordered phase, with evidence of polaronic transport both above and *below* T_c, as reported separately. The magnetic behaviour presented below contrasts with comparable levels of Ca doping which produce a canted antiferromagnetic ground state, reminiscent of the undoped host [12]. To date the effects of Mg substitution have received relatively little attention, and while the comparatively small size of these ions—with attendant modifications to the Mn–O–Mn bond angle—will likely play a significant role, the precise origin of such differences are not currently understood.

2. Experimental details

Samples of $La_{0.95}Mg_{0.05}MnO_3$ (nominal) were prepared by conventional ceramic techniques. Stoichiometric quantities of ultra-pure La_2O_3, MgO (type FM) and MnO_2 (99%) were mixed for 24 hours by ball-milling in acetone. The resulting dried powder was pressed into pellet form and heated in air at 800 °C for 24 hours. Such preheated samples were hand ground with a binder (polyvinyl alcohol in water) in a mortar and pestle, granulated and pressed into a disc shape. The latter were then sintered for 48 hours in air at 1200 °C. Room temperature x-ray diffraction using Cu Kα radiation was collected from $2\theta = 20$ to 80° in steps of 0.05° using an automated Philips PW 1710 system incorporating a Bragg–Brentano goniometer equipped with incident and diffracted beam Soller slits. These data confirmed the presence of a single phased orthorhombic structure ($Pbnm$) with $a = 5.4907$ Å, $b = 5.7097$ Å and $c = 7.7254$ Å, i.e. $c/\sqrt{2} < a < b$ as expected. Furthermore there were no indications of impurity phases above background, in particular the oxides of manganese.

Magnetic measurements were performed on a sample of approximate dimensions ($0.8 \times 1.3 \times 7$) mm^3. Dc magnetization and ac susceptibility data were acquired as a function of both temperature and field in a Quantum Design PPMS model 6000 system.

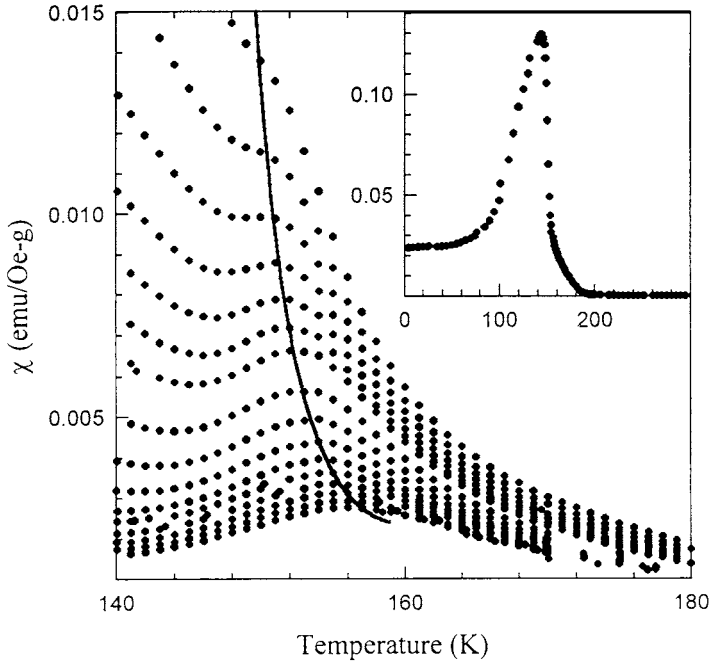

Figure 1. The field- and temperature-dependent ac susceptibility (corrected for background and demagnetizing effects) plotted against temperature for applied fields ranging from 400 to 3000 Oe. The inset shows the behaviour of the zero-field susceptibility.

3. Results and discussion

3.1. Susceptibility

The inset in figure 1 displays the zero-field susceptibility $\chi_0(T)$ (measured on warming at 2.4 kHz with a driving field amplitude of 30 mOe) as a function of temperature. With decreasing temperature $\chi_0(T)$ increases rapidly as the ferromagnetic transition temperature T_c ($\sim$150 K) is approached from above, peaking at the Hopkinson maximum, and then decreases monotonically as the temperature is further lowered. The Hopkinson or principal maximum is not critical in origin—it derives from processes controlling the regular/technical contributions in this response [13] rather than the singular contributions—and the peak susceptibility here represents some 60% of the limit set by demagnetization constraints (estimated in figure 3), a point discussed in more detail below. The singular component in the response is examined in detail in the main body of figure 1. Here the ac susceptibility is plotted against temperature in a range of superimposed static biasing fields between 400 and 3000 Oe (both the static and the ac driving field were applied along the largest sample dimension). The effects of such static fields are to suppress the Hopkinson maxima in both amplitude and temperature so that secondary critical maxima can be resolved, as reported in a variety of other systems [10, 14]. As is evident in this figure, these critical maxima decrease in amplitude but shift upwards in temperature from T_c as the static field increases, in agreement with theoretical expectations discussed previously [15]. In particular magnetic critical exponents can be estimated *directly* from such maxima rather than relying on extrapolation techniques (to zero field) implicit in

conventional approaches. In essence, the static scaling law equation of state [16]

$$m(h,t) = t^{\beta} F\left(\frac{h}{t^{\gamma+\beta}}\right) \qquad \chi(h,t) = \frac{\partial m}{\partial h} = t^{-\gamma} G\left(\frac{h}{t^{\gamma+\beta}}\right) \tag{1}$$

relates the (reduced) magnetization (m) to the usual linear scaling fields $t = |T - T_c|/T_c$ and $h \sim H_{int}/T_c$ in the vicinity of T_c, where H_{int} is the *internal* field. Utilizing the Widom equality, $\gamma = \beta(\delta - 1)$, enables the field dependent susceptibility to be rewritten as

$$\chi(h,t) = t^{-\gamma} G\left(\frac{h}{t^{\gamma+\beta}}\right) = h^{(\delta-1)/\delta} H\left(\frac{h}{t^{\gamma+\beta}}\right) \tag{2}$$

where G is the derivative of the (unspecified) scaling function F with respect to its argument (X), and $H(X) = X^{\gamma/(\gamma+\beta)} G(X)$. From equation (2) it follows directly that the susceptibility data acquired in fixed field (so that the prefactor $h^{(\delta-1)/\delta}$ is constant) as a function of temperature yield the functional dependence of $H(X)$ directly [14] (through variations in the denominator of X). More important, since the scaling approach is based on the premise that $H(X)$ and the other scaling functions exhibit a universal dependence on their argument X, then any feature they exhibit—specifically the maxima evident in figure 1—occur at the *same* value of this argument. Consequently, with $t_m = (T_m - T_c)/T_c$ representing the reduced temperature of such maxima,

$$\frac{h}{t_m^{\gamma+\beta}} = X_m \qquad t_m \propto h^{1/(\gamma+\beta)} \tag{3}$$

where X_m denotes the (constant) argument of these functions (F and G, as well as H) at the maxima. As a corollary [14] (as the function $G(X_m)$ is also a constant, for a fixed argument), then from equation (1)

$$\chi(h, t_m) \propto h^{(\delta-1)/\delta} \tag{4}$$

and

$$\chi(h, t_m) \propto t_m^{-\gamma}. \tag{5}$$

Equations (3), (4) and (5) thus allow the exponents γ, β and δ to be determined *directly* from the peak structure evident in figure 1, as detailed below. Physically the line in the (H–T) plane delineated by these maxima—the crossover line (hence the designation of ($\gamma + \beta$) as the crossover exponent)—separates the 'high' temperature region in which the response is thermally dominated from a lower temperature regime in which it is field dominated, as explained qualitatively by the fluctuation–dissipation theorem [17]. Figure 2 reproduces a double logarithmic plot of the critical peak amplitude $\chi(h, t_m)$ (corrected for background and demagnetizing effects) against the internal field H_{int} ($H_{int} = H_a - NM$ (in conventional notation) was found from the measured magnetization (M) and the slope, N^{-1}, of the low field 'shearing' curves near T_c, figure 3). The straight line drawn in this figure, a least squares fit to these data, confirms the power-law prediction—equation (4)—and the slope yields

$$\delta = 4.75 \pm 0.15$$

($400 \leqslant H_{int} \leqslant 3$ kOe). The latter is close to the value predicted ($\delta = 4.80$) by renormalization group calculations for the nearest neighbour, isotropic three-dimensional Heisenberg model [18]. In a similar manner figure 4 confirms the applicability of equation (3); the straight line, least squares fit shown yields

$$\gamma + \beta = 1.75 \pm 0.05$$

($400 \leqslant H_{int} \leqslant 3$ kOe) in excellent agreement with Heisenberg model predictions [18]. Plots of t_m of course require a value for T_c to be specified; this was done by plotting the T_m

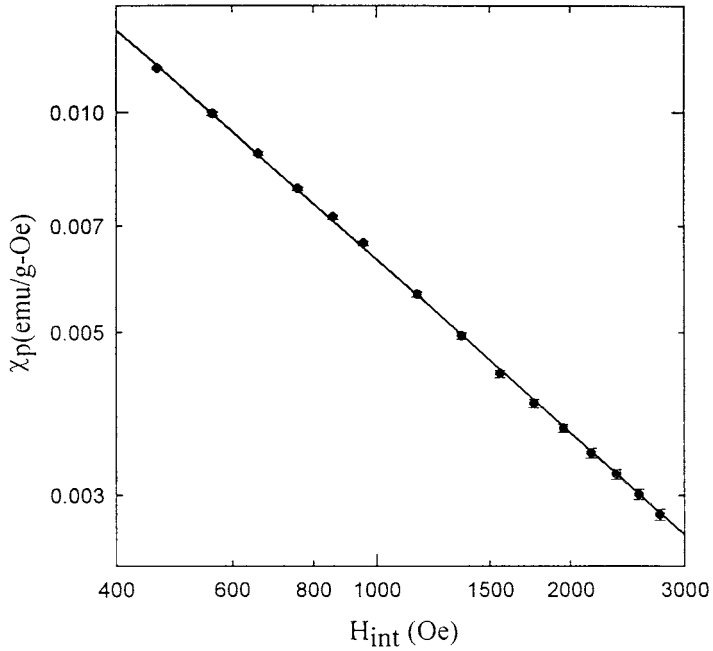

Figure 2. The peak/maximum susceptibility, $\chi_p = \chi(h, t_m)$ taken from data similar to those shown in the main body of figure 1, plotted against the internal field on a double logarithmic scale. The straight line confirms the power law prediction of equation (4) and yields a value of $\delta = 4.75$ (± 0.15).

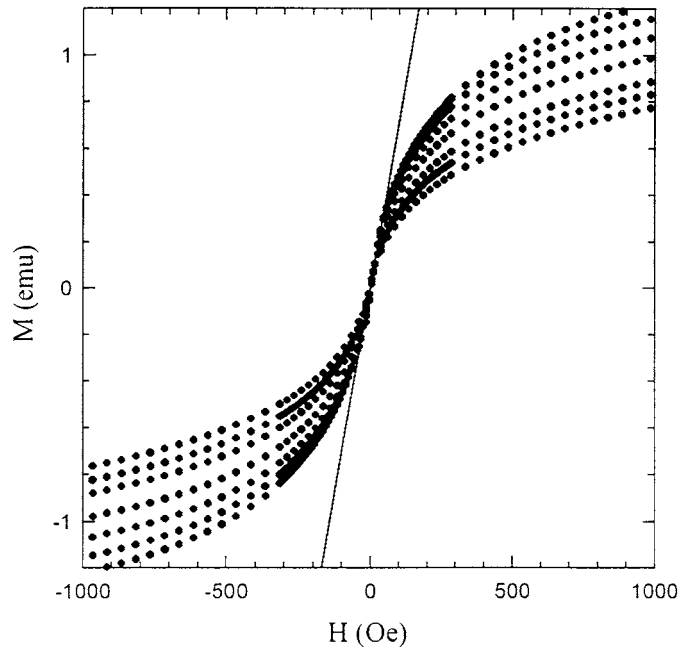

Figure 3. Plots of the sample magnetization against the applied field for temperatures between 138 and 148 K—so-called shearing curves. The line drawn is used to estimate the demagnetization factor.

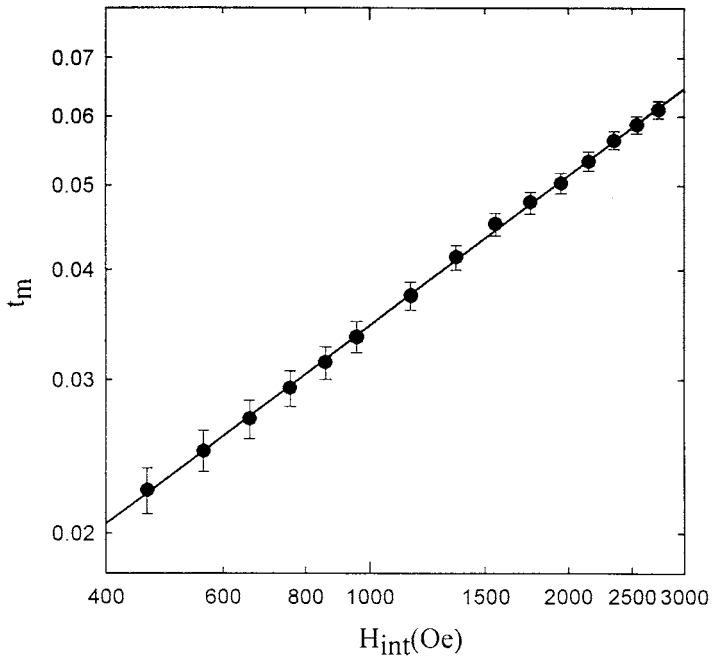

Figure 4. A plot of the susceptibility of the peak temperature (taken from figure 1) against the corresponding internal field on a double logarithmic scale. The straight line confirms the power law prediction of equation (3) and yields $\gamma + \beta = 1.75$ (± 0.05).

estimates (taken directly from data similar to those shown in figure 1) against $H_{int}^{1/\gamma+\beta}$, with an extrapolation of the ensuing linear behaviour yielding an estimate for T_c. While such plots have been made with a range of exponent values, the best fit was obtained for values close to the predicted Heisenberg model estimates and yielded $T_c = 147.2 \pm 0.2$ K, a value also confirmed via figure 4. In this system T_c is closer to the Hopkinson maximum than in most other systems studied previously, being only some 1.5 degrees higher in temperature. A further comparison with predicted exponent values is made in figure 5, a double logarithmic plot of the peak susceptibility $\chi(h, t_m)$ (corrected for background and demagnetizing effects) against t_m; here—from the straight line, least squares fit shown—we find

$$\gamma = 1.39 \pm 0.03$$

($t_m \geqslant 2 \times 10^{-2}$) compared with a model predicted value of 1.386.

While such an approach yields estimates for these exponents in a very direct manner, figures 5 (inset) and 6 offer comparisons with conventional approaches. Figure 6 reproduces the magnetization as a function of (internal) field along the critical isotherm ($T = T_c$, $M \propto H_{int}^{1/\delta}$); from the line drawn on this double logarithmic plot δ is estimated as

$$\delta = 4.80\ (\pm 0.2)$$

(1 kOe $\leqslant H_{int} \leqslant$ 10 kOe), which agrees—uncertainties in both the estimate for T_c and the reliability of resetting the measuring temperature to this estimate notwithstanding—with the value deduced above from figure 2 (which is *independent* of the choice for T_c). The inset in figure 5 shows the temperature dependence of the effective Kouvel–Fisher susceptibility exponent [19] deduced directly from the zero-field susceptibility, *viz.*

$$\gamma^*(t) = \mathrm{d}(\ln \chi(0, t))/\mathrm{d} \ln(t).$$

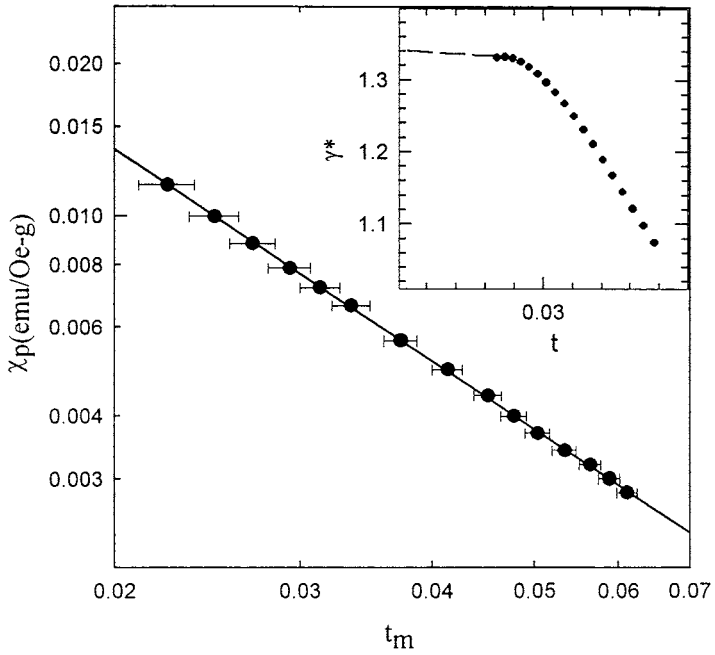

Figure 5. The peak/maximum susceptibility, $\chi_p = \chi(h, t_m)$ plotted against the reduced peak temperature on a double logarithmic scale, verifying the power law of equation (5). The slope of the line drawn yields $\gamma = 1.39$ (± 0.05). The inset reproduces the temperature dependence of the effective Kouvel–Fisher susceptibility exponent discussed in the text.

For temperatures $t \geqslant 3 \times 10^{-2}$, this effective exponent falls with increasing temperature from a value of $\sim$1.34 towards a mean-field value of 1.0, as expected [20]. Below $t \sim 3 \times 10^{-2}$ the failure of the zero-field susceptibility to climb towards the demagnetization-factor-limited value precludes a reliable estimate of $\gamma^*(t)$ to be found from $\chi(0, t)$ in this region, a point discussed in more detail below. The dashed line drawn in this inset for lower temperatures connects these $\gamma^*(t)$ data with the Heisenberg model value found above from the field-dependent susceptibility peak data.

In summary, the magnetic critical exponent values deduced over the field and temperature ranges indicated are completely consistent with Heisenberg model predictions, and with expectations emanating from the fully three-dimensional characteristics of the extreme ($n = \infty$) members of the Ruddlesden–Popper series. These results conflict with those reported for some Sr-doped perovskites [21, 22] but not with measurements on a Mg-doped perovskite with $x \simeq 0.33$ [10] and the pyrochlore system [14] $Tl_2Mn_2O_7$.

The above conclusions warrant further comment, first with regard to $\chi_0(T)$ not reaching the limit set by demagnetization constraints, and second the true, asymptotic nature of the exponent estimates. Since the first point has been addressed in some detail previously [23], the principal points alone are repeated here. At the demagnetization limit the internal field H_{int} ($= H_a - NM$) is zero. In an ac measurement this requires not only that the magnetization oscillates (reverses), but also that the amplitude of such oscillations increases as N decreases in order to maintain this condition. Correspondingly, any process which inhibits this reversal is more readily revealed by measurements on small N specimens (here N is close to an order of magnitude smaller than for a sphere). The probable inhibiting mechanism here is single-ion spin–orbit coupling at Mn^{3+} (Jahn–Teller) sites. The second issue concerns the approach of

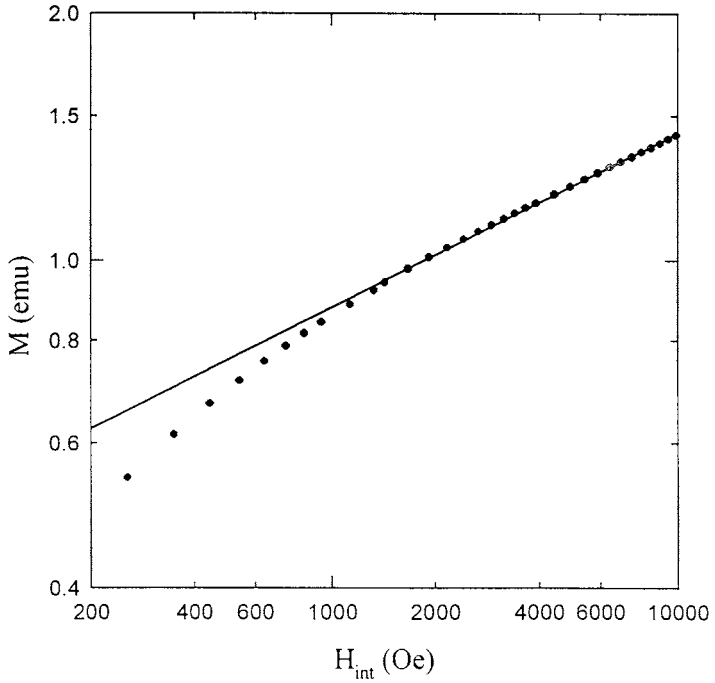

Figure 6. The sample magnetization measured along the critical isotherm plotted against the internal field. The line drawn corresponds to $\delta = 4.80$ (± 0.2).

the present data to the critical point ($h \rightarrow 0$, $t \rightarrow 0$), and the true, asymptotic nature of the exponent estimates; this requires more extensive discussion. The quoted γ value of 1.39 ± 0.05 was extracted from data for which $t \geqslant 2 \times 10^{-2}$; while this reduced temperature is comparable to that used in many other studies, it is still at least an order of magnitude further from the critical point than some of the 'best' estimates [24] (although it should be pointed out that this difference can be attributed, in part, to the relatively low T_c value here). By contrast the data included in figure 2 extend down to 400 Oe, which is closer to the asymptotic limit ($h \rightarrow 0$) than is usual for conventional estimates for δ (critical isotherm data below 1 kOe are seldom utilized). Nevertheless, exponent estimates based on the field and temperature variation of the susceptibility maxima have, under the most favourable conditions [25], been extended down to fields some three orders of magnitude smaller than those reported here, i.e. critical peak structure has been resolved in fields of only $\sim$0.4 Oe. The possible origin of such differences is next discussed.

In metallic systems the most favourable conditions referred to above have been linked to the absence of both an orbital moment and (through spin–orbit coupling) an associated (single-ion) anisotropy. Specifically, fitting equations (3) and (4) to experimental data and extracting meaningful exponent values from such fits relies on the assumption that the measured response is dominated by the singular contribution (on which such equations are based), as indeed do more conventional approaches. An examination of previous data has revealed that this requirement is most readily achieved in materials not only with a low net moment, but also in which the non-critical/regular component (typically associated with domain wall motion, coherent rotation etc) is easily saturated (*viz.* technical saturation is achieved in relatively low applied fields). Since the Hopkinson maximum originates from these regular

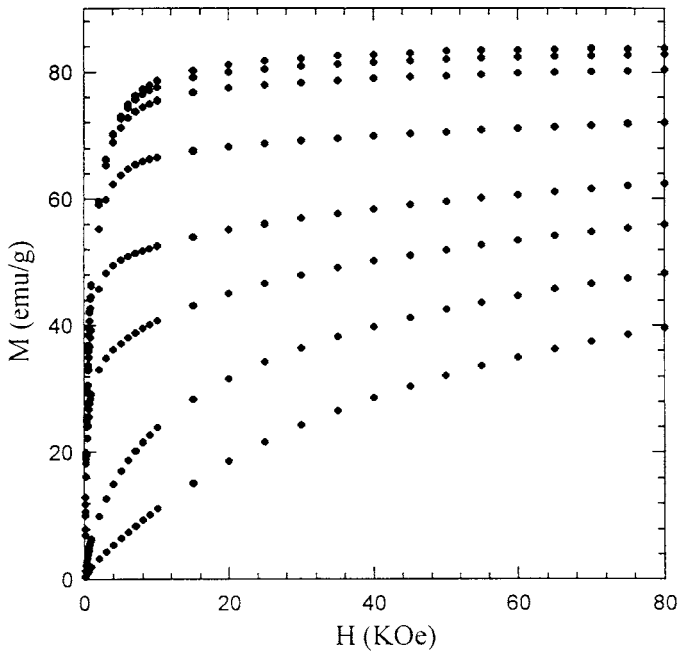

Figure 7. Sample magnetization plotted against applied field at fixed temperatures of 4.2 K (top), 20 K, 40 K, 80 K, 120 K, 140 K, 160 K and 180 K (bottom).

processes it is rapidly suppressed in amplitude and temperature by modest fields in such systems; this enables the critical maxima to be resolved, a feature identified with the onset of the applicability of equations (3) and (4). This does not happen here. At first sight the presence of Mn^{3+} ions (a Jahn–Teller ion with spin–orbit mediated anisotropy) appears to provide a ready explanation of this result. Closer inspection however reveals difficulties with it.

The coercive field H_c provides a direct measure of the processes opposing magnetization reversal at any temperature. Figure 7 reproduces magnetization curves acquired for the present system at a variety of temperatures, and figure 8 displays the temperature dependence of the coercive field $H_c(T)$ deduced from the hysteresis loops. The dashed line represents the experimental data, and the solid line represents a theoretical calculation to be discussed later. The measured $H_c(T)$ falls from a value of $\sim$65 Oe in the liquid helium range to zero at T_c; in particular at some 10 K below T_c measurements show $H_c(T) \leqslant 10$ Oe. In many systems studied previously [14], applied fields of typical magnitude $H_c(T \leqslant T_c)$ have been found to saturate the (regular) component arising from technical contributions thus enabling critical peak structure to be resolved. This does not occur here, nor in several other doped perovskite [10, 26, 27] and pyrochlore [14] systems studied using the present techniques. An examination of figure 7 reveals the source of this difference; it is not the relative magnitude of the applied field H_a and the coercive field $H_c(T)$ but rather the persistence of a significant higher field slope in these magnetization curves. The latter indicates a substantial reversible contribution to the (technical) magnetization process at fields well beyond $H_c(T)$. Before discussing possible origins for such a large reversible component—and its influence on the apparent value of the coercive field—we examine the magnetization data in more detail.

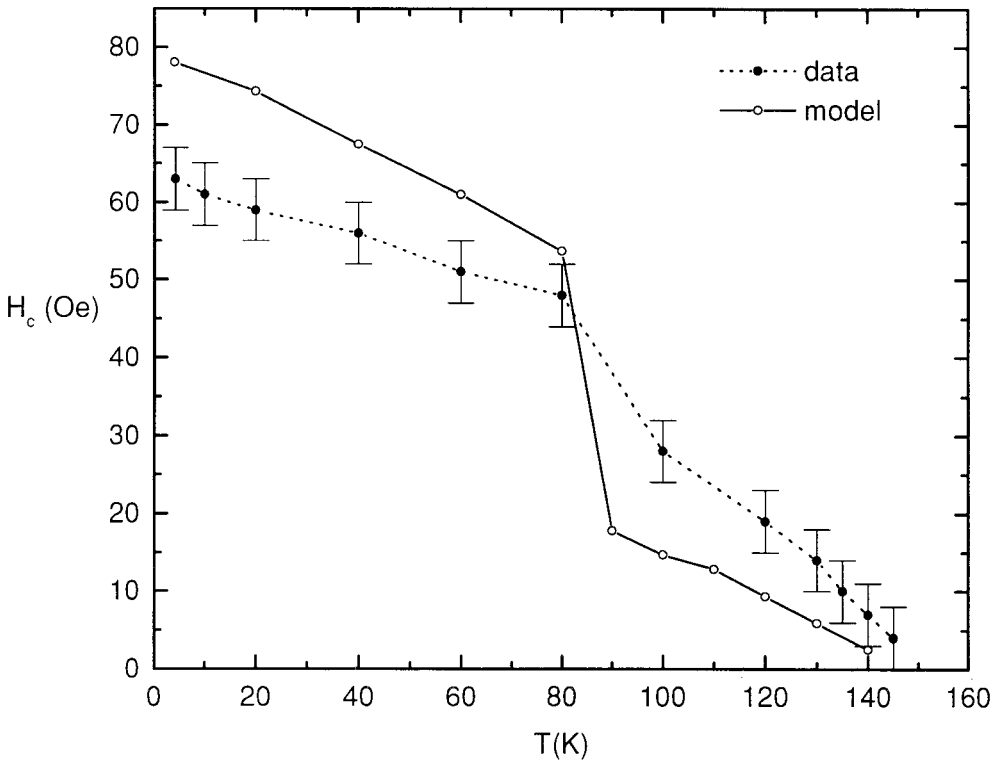

Figure 8. The temperature dependence of the measured coercivity $H_c(T)$ of $La_{0.95}Mg_{0.05}MnO_3$ (dashed line) and of the coercivity calculated by the Preisach model (solid line).

3.2. Magnetization

Figure 9 shows the temperature dependence of the FC and ZFC response measured in an applied field $H_a = 10$ Oe. The discrete points are the experimental data and the solid curves are theoretical fits to be described later. The ZFC data were acquired by first cooling the sample from $T = 300$ K to $T = 4.2$ K in zero applied field, then turning on the field $H_a = 10$ Oe and warming. The FC data were taken by cooling from $T = 300$ K in the applied field $H_a = 10$ Oe and then warming from $T = 4.2$ K. The FC and ZFC branches are identical above $T_c \simeq 150$ K, but exhibit a strong bifurcation just below T_c, indicative of the onset of irreversibility and hysteresis. While the FC data are relatively featureless, the ZFC response exhibits unusual structure with increasing temperature in the form of a relatively abrupt jump near $T \cong 85$ K, followed by a weak maximum just below T_c. Within the magnetically ordered phase below T_c, the FC and ZFC response are dominated by technical magnetization processes related to domain wall motion and moment rotation, and the Preisach model of hysteresis provides a formal theoretical framework for analysing and interpreting this irreversible component of the magnetic response.

The Preisach model [28, 29] decomposes all magnetic systems into a collection of many bistable subsystems. In the original form of the model [28], each subsystem is characterized by a rectangular response function like that shown in figure 10(a), with two states $\phi = \pm\mu$, corresponding to the two discrete orientations of the subsystem moment μ, and two critical instability fields (H_+, H_-), with $H_- < H_+$, which can be decomposed into a *coercive* field

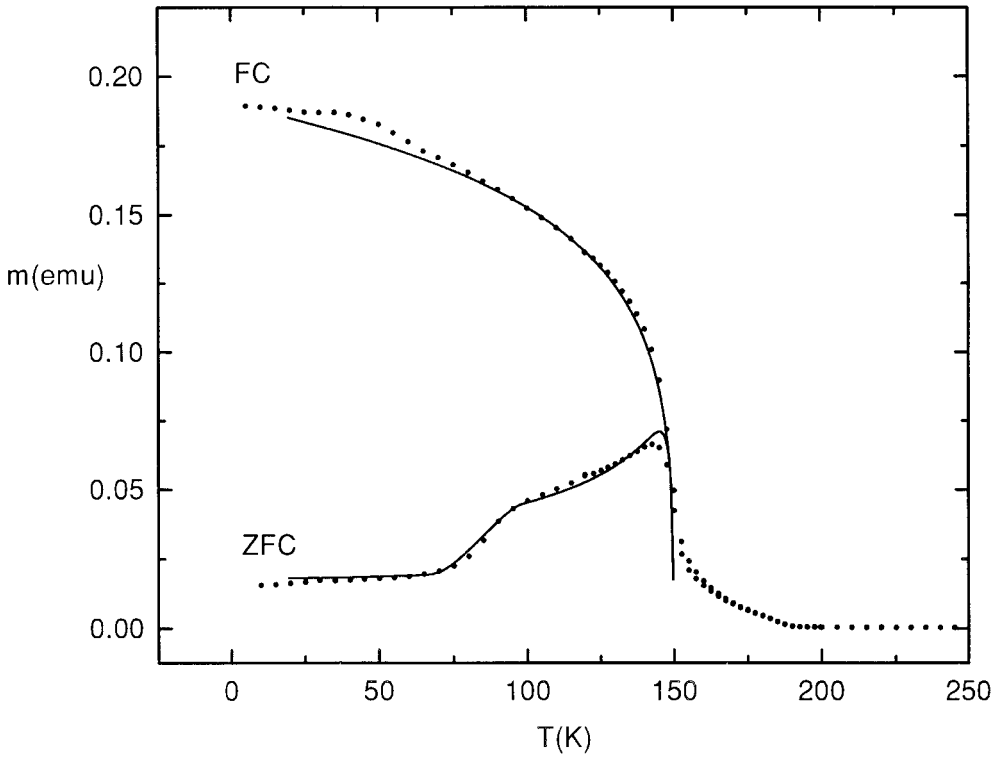

Figure 9. The temperature dependence of the field-cooled (FC) and zero-field-cooled (ZFC) response of $La_{0.95}Mg_{0.05}MnO_3$ measured in a nominal applied field $H_a = 10$ Oe. The solid curves are Preisach simulations described in the text.

$H_c = (H_+ - H_-)/2$ and an *asymmetry* field $H_i = -(H_+ + H_-)/2$. In more fundamental terms, each subsystem represents an 'elementary' fragment of the free energy landscape, which satisfies the minimum requirements to exhibit metastability and hysteresis. The equivalent zero-field energy level diagram of a subsystem, shown in figure 10(b), is an asymmetric double well potential, with two energy barriers $W_- = -\mu H_- = \mu(H_c + H_i)$ and $W_+ = \mu H_+ = \mu(H_c - H_i)$ which inhibit transitions between the two valleys and block moment reorientation. The coercive field H_c functions like an *intrinsic anisotropy field*, which stabilizes the two moment orientations $\phi = \pm\mu$, and measures the *energy dissipated* as heat in a transition [29], while the asymmetry field H_i plays the role of a *local interaction field* due to neighbouring subsystems, which lifts the degeneracy of the two valleys, and measures the *energy stored* in a transition [29]. The Preisach approach assumes that all such regions have the *same moment*, but are distinguished from each other by their characteristic coercive and interaction fields, which are distributed among the subsystems according to a probability density $p(H_c, H_i)$, which is typically assumed to be the product of two Gaussians $p(H_c, H_i) = (2\pi\sigma_c^2)^{-1/2}\exp[-(H_c - \bar{H}_c)^2/2\sigma_c^2](2\pi\sigma_i^2)^{-1/2}\exp[-H_i^2/2\sigma_i^2]$. The model has recently been generalized [30] to include *thermal overbarrier relaxation effects*, which are described by an effective thermal viscosity field $H_T^* = (k_B T/\mu)\ln(t_{exp}/\tau_0)$ (where t_{exp} is the experimental time constant and τ_0 is a microscopic time), and *critical effects* related to the existence of a critical ordering temperature T_c, by allowing the spontaneous moment μ and

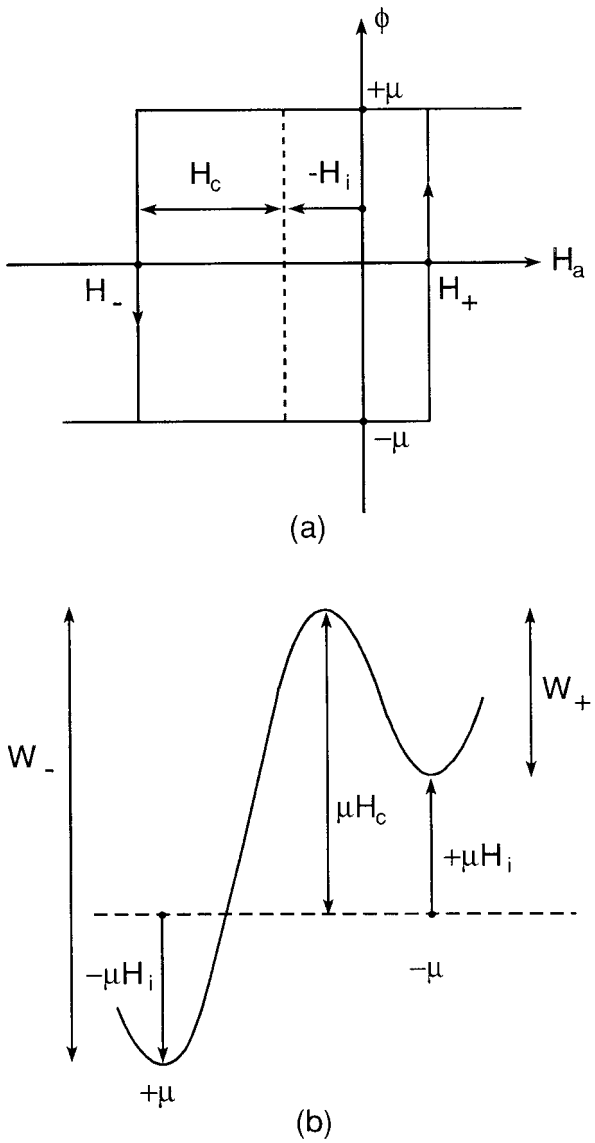

Figure 10. (a) The rectangular response function for an elementary Preisach subsystem with states $\phi = \pm\mu$, coercive field H_c, interaction field H_i and switching fields H_+ and H_-. (b) The zero-field energy level diagram for the Preisach subsystem in (a). W_+ and W_- are the excitation energies for transitions between the states $\phi = \pm\mu$.

the Preisach distribution parameters to vary as powers of the reduced temperature $(1-T/T_c)$ as:

$$\left\{\begin{array}{c} \mu = \mu_0(1-T/T_c)^{\Gamma} \\ \bar{H}_c = \bar{H}_{c0}(1-T/T_c)^{\Gamma_c} \\ \sigma_c = \sigma_{c0}(1-T/T_c)^{\Gamma_c'} \\ \sigma_i = \sigma_{i0}(1-T/T_c)^{\Gamma_i} \end{array}\right\}.$$

The parameter Γ plays the same role as the critical exponent β employed in the critical analysis, although, for reasons of computational simplicity, we assume here that the power

Table 1. Preisach model fitting parameters.

μ_0 (emu)	$\tilde{H}_{c01}$ (Oe)	σ_{c01} (Oe)	$\tilde{H}_{c02}$ (Oe)	σ_{c02} (Oe)	σ_{i0} (Oe)	Γ	Γ_c	Γ'_c	Γ_i
1.0×10^{-13}	120	60	1.2	48	12.6	0.45	0.45	0.22	0.28
T_c (K)	T_0 (K)	H_a (Oe)	M_0 (emu)	f	$\Omega = \ln(t_{exp}/\tau_0)$	λ			
150	85	8.4	0.35	0.89	25	0.000 85			

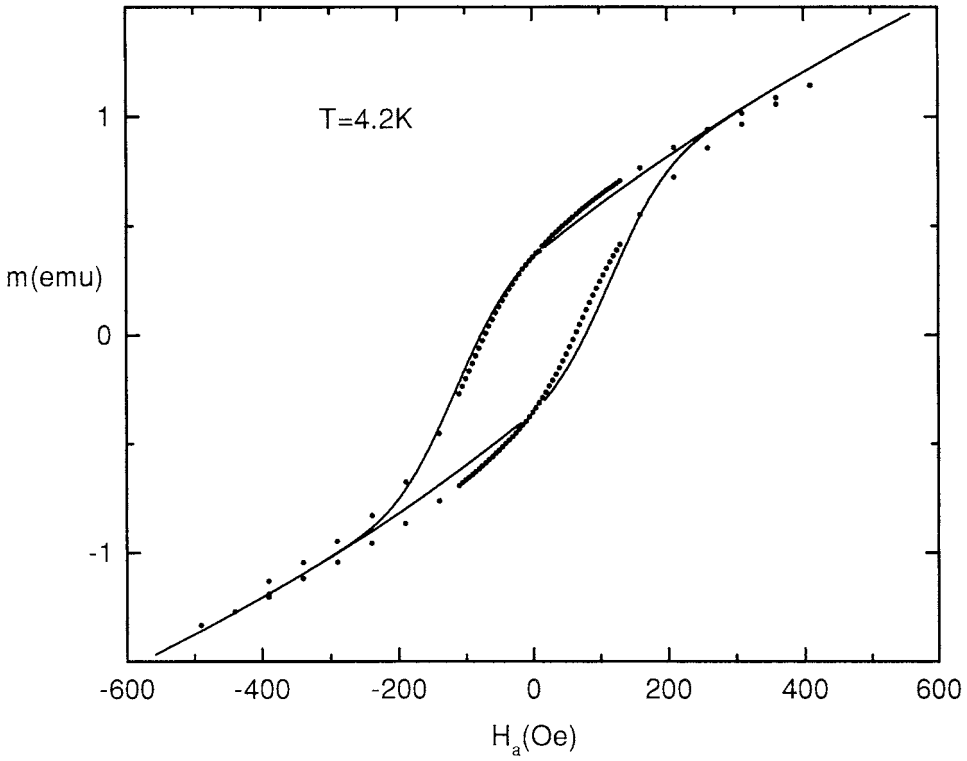

Figure 11. The major hysteresis loop of $La_{0.95}Mg_{0.05}MnO_3$ measured at $T = 4.2$ K (discrete points) and the calculated Preisach loop (solid curves) as described in the text.

law $(1 - T/T_c)^{\Gamma}$ is valid for *all* $T \leqslant T_c$. The model provides explicit constructions and elegant mathematical algorithms for replicating FC and ZFC processes and hysteresis loops, as described in detail in the literature [30].

The solid curves in figure 9 are numerical simulations of the FC and ZFC response generated from the extended version of the Preisach model described above, and the best fit model parameters are listed in table 1. These same parameters were also used to generate hysteresis loops over a wide range of temperatures $T < T_c$, and figure 11 shows a typical comparison of the measured (discrete points) and calculated (solid curves) major loops at $T = 4.2$ K. Estimates of the model coercive field H_c were extracted from the loop simulations, and figure 8 shows a comparison of the temperature dependence of the measured coercivity (dashed line) and the coercivity predicted by the simulations (solid line). Although the number of fitting parameters is large, several of these parameters (such as the critical temperature T_c, the characteristic temperature T_0 which defines the 'step' in the ZFC moment, the applied

field H_a, the saturation moment M_0 and the experimental time parameter Ω) are essentially fixed by the experimental data and conditions, and are relatively inflexible. Furthermore, many of the remaining parameters are also 'robust' in the sense that their influence is limited primarily to one very particular structural feature of the experimental data, so that their values are accordingly highly reliable.

These fits offer considerable insight into the technical magnetization processes which characterize the $LaMgMnO_3$ system. In particular, our analysis shows that the 'step' in the ZFC moment in figure 9 in the vicinity of $T_0 = 85$ K is a manifestation of a crossover between two regimes with distinct anisotropy characteristics: a low temperature regime ($T < 85$ K), described by a Gaussian distribution of coercive fields with a zero-temperature mean $\bar{H}_{c01} = 120$ Oe and a zero-temperature dispersion $\sigma_{c01} = 60$ Oe, and a magnetically 'softer' high temperature regime, described by a highly truncated Gaussian ($\bar{H}_{c02} = 1.2$ Oe, $\sigma_{c02} = 48$ Oe) with a true mean $\langle H_{c02} \rangle_{true} = 20$ Oe which is significantly lower than $\bar{H}_{c01}$. This crossover at $T_0 = 85$ K is clearly visible in the temperature dependence of the calculated coercivity in figure 8, and is coincident with a similar although somewhat weaker structural anomaly in the measured coercivity.

The other feature of these fits which deserves special attention is the necessity to supplement the Preisach calculation by a large reversible term, so that the total system response is described by $M = M_0[(1 - f)(\text{Preisach}) \pm f(1 - \exp(-\lambda|H_a|))]$. As table 1 shows, the reversible contribution accounts for roughly 90% of the total system response ($f = 0.89$), and its effects are noticeable even in the low field ($H_a = 10$ Oe) response in figure 9 as a finite positive offset in the ZFC moment at $T = 0$. It is precisely this combination of a large reversible component superimposed on a smaller hysteretic contribution that results in the system appearing softer than its 'intrinsic' response. This can be seen directly in the parameters of the model calculation—a zero-temperature mean coercive field $\bar{H}_{c01} = 120$ Oe produces a predicted coercivity of about 80 Oe when combined with the reversible contribution. This feature accounts qualitatively—if not quantitatively—for the appearance of a technical hardness irreconcilable with the measured low coercive field values.

A possible origin for this reversible or non-saturating regular contribution was recently discussed [26] for $La_{0.67}Ca_{0.33}MnO_3$. In the intrinsically inhomogeneous mixed valent (Mn^{3+}–Mn^{4+}) state of systems of this latter type, double exchange and the associated ferromagnetic (critical) fluctuations would predominate in those regions statistically rich in the substituted cation, whereas other regions statistically diminished in the divalent dopant species would be expected to display antiferromagnetic correlations characteristic of Mn^{3+}–Mn^{3+} (t_{2g}–$O(2p_\pi)$–t_{2g}) superexchange in the undoped parent compound. While the former dominates the overall critical behaviour, contributions from the latter could still play a significant role. In particular, since the uniform applied field H_a is the appropriate conjugate field for ferromagnetic—but not antiferromagnetic—order, the incipient fluctuations associated with the latter order would be suppressed by an increasing H_a, and as such the associated contribution to the measured response would be reminiscent of a regular (not *ferromagnetic* critical) response, as argued previously [26].

While such a model has several features which are consistent with observations, it cannot reproduce in any direct way the anomalies observed in the ZFC and FC moments or in the temperature dependence of $H_c(T)$. These data therefore cannot be used as support for models predicting electronic phase separation in the temperature regime below T_c as have recent FC data on $La_{1-x}Ca_xMnO_3$ exhibiting similar features, as there additional NMR measurements played a crucial role [31]. Furthermore, while the microscopic nature of the statistically inhomogeneous approach holds some appeal, a phenomenological macroscopic model—consistent with the philosophy of the Preisach approach—cannot be discounted. The model

data used in figure 9 attributes a moment of about 10^{-13} emu (about 3×10^6 Mn atoms) to reversing (Barkhausen) entities involved in the hysteresis process, with roughly 10^7 such entities in an average grain (typical size 40 μm). A possible macroscopic picture would thus consist of hysteretic processes associated with moment (10^7 μ_B) reversal near the surface of grains with large elastic (reversible) domain wall motion occurring in the main body of a grain.

Irrespective, however, of the actual origin of the reversible component in the response, it is the essential element complicating the behaviour of these systems.

4. Conclusions

Analysis of the measured response of the $La_{0.95}Mg_{0.05}MnO_3$ system near the paramagnetic to ferromagnetic transition temperature $T_c = 147.2 \pm 0.2$ K yields exponent values of $\gamma = 1.39 \pm 0.05$, $\gamma + \beta = 1.75 \pm 0.05$ and $\delta = 4.75 \pm 0.15$, consistent with Heisenberg model predictions and the fully three-dimensional nature of this $n = \infty$ Ruddlesden–Popper compound. This system—along with several other doped manganese perovskites and some pyrochlores—also displays a large reversible component in the magnetic response at and below T_c which complicates analysis of this critical behaviour. Possible origins for this reversible component are discussed.

Acknowledgments

Support for this work from both the Natural Sciences and Engineering Research Council (NSERC) of Canada and the University of Manitoba (in the form of graduate fellowships to J H Zhao and T Song) is gratefully acknowledged.

References

[1] Jonkers G H and van Santen J H 1950 *Physica* **16** 337
van Santen J H and Jonkers G H 1950 *Physica* **16** 599
Searle C W and Wang S T 1969 *Can. J. Phys.* **47** 2703
Searle C W and Wang S T 1970 *Can. J. Phys.* **48** 2023
[2] Parkin S S 1995 *Ann. Rev. Mater. Sci.* **25** 357
[3] Okomoto Y, Katsufuji T, Ishikawa T, Arima T and Tokura Y 1997 *Phys. Rev.* B **55** 4206
Matl P, Ong N P, Yan Y F, Li Y Q, Studebaker D, Baum T and Doubinina G 1998 *Phys. Rev.* B **57** 10 248
[4] Ruddlesden S N and Popper P 1958 *Acta Crystallogr.* **11** 541
[5] Zener C 1951 *Phys. Rev.* **81** 440
Anderson P W and Hasegawa H 1955 *Phys. Rev.* **100** 675
[6] Millis A J, Littlewood P B and Shraiman B I 1995 *Phys. Rev. Lett.* **74** 5144
Millis A J, Shraiman B J and Mueller R 1996 *Phys. Rev. Lett.* **77** 175
Li Q, Zang J, Bishop A R and Soukoulis C M 1997 *Phys. Rev.* B **56** 4541
[7] Hibble S J, Cooper S P, Hannon A C, Fawcett I D and Greenblatt M 1999 *J. Phys.: Condens. Matter* **11** 9221
[8] Alexandrov A S and Bratkovsky A M 1998 *Phys. Rev. Lett.* **82** 141
Alexandrov A S and Bratkovsky A M 1999 *J. Phys.: Condens. Matter* **11** 1989
Alexandrov A S and Bratkovsky A M 1999 *J. Phys.: Condens. Matter* **11** L531
[9] Schiffer P, Ramirez A P, Bao W and Cheong S-W 1995 *Phys. Rev. Lett.* **75** 3336
Tomioka Y, Asamitsu A, Kuwahara H, Morimoto Y and Tokura Y 1996 *Phys. Rev.* B **53** R1689
[10] Zhou X Z, Kunkel H P, Zhao J-H, Stampe P A and Williams G 1997 *Phys. Rev.* B **56** R12 714
[11] Zeng Z, Greenblatt M, Subramanian M A and Craft M 1999 *Phys. Rev. Lett.* **82** 3164
[12] Hennion M, Moussa F, Rodriguez-Carvajal J, Pinsard L and Revcolevschi A 1997 *Phys. Rev.* B **56** R497
Hennion M, Moussa F, Biotteau G, Rodriguez-Carvajal J, Pinsard L and Revcolevschi A 1998 *Phys. Rev. Lett.* **81** 1957

[13] Chikazumi S 1997 *Physics of Ferromagnetism* 2nd edn (Oxford: Clarendon) p 486
[14] Zhao J-H, Kunkel H P, Zhou X Z, Williams G and Subramanian M A 1999 *Phys. Rev. Lett.* **83** 219
Stampe P A and Williams G 1998 *J. Phys.: Condens. Matter* **10** 6771
Williams G 1991 *Magnetic Susceptibility of Superconductors and Other Spin Systems* ed R A Hein *et al* (New York: Plenum) p 475 *et seq*
[15] Roshko R M and Williams G 1984 *J. Phys. F: Met. Phys.* **14** 703
[16] Stanley H E 1971 *Introduction to Phase Transitions and Critical Phenomena* (Oxford: Clarendon)
[17] Kunkel H P, Roshko R M and Williams G 1988 *Phys. Rev.* B **37** 5880
[18] Le Guillon L C and Zinn-Justin J 1980 *Phys. Rev.* B **21** 3976
[19] Kouvel J S and Fisher M E 1964 *Phys. Rev.* A **136** 1626
[20] Souletie J 1987 *J. Physique* **49** 1211
Fähnle M and Souletie J 1985 *J. Phys. C: Solid State Phys.* **17** L469
Fähnle M and Souletie J 1985 *Phys. Rev.* B **32** 3328
[21] Ghosh K, Lobb C J, Greene R L, Karabashev S G, Shulyater D A, Arsenov A A and Mukovskii Y 1998 *Phys. Rev. Lett.* **81** 4740
[22] Mohan Ch V, Seeger M, Kronmuller H, Murugaraj P and Maier J 1998 *J. Magn. Magn. Mater.* **183** 348
[23] See the discussion on the response of the CuNi system [14] and Wang Z, Kunkel H P and Williams G 1990 *J. Phys.: Condens. Matter* **2** 4173
[24] Kaul S N 1988 *J. Phys. F: Met. Phys.* **18** 2089
Kaul S N and Mohan C V 1994 *Phys. Rev.* B **50** 6157
[25] Wang Z, Kunkel H P and Williams G 1992 *J. Phys.: Condens. Matter* **4** 10 385
[26] Zhao J H, Zhou X Z, Peles A, Ge S, Kunkel H P and Williams G 1999 *Phys. Rev.* B **59** 8391
[27] Peles A, Kunkel H P, Zhou X Z and Williams G 1999 *J. Phys.: Condens. Matter* **11** 8111
[28] Preisach F 1935 *Z. Phys.* **94** 277
[29] Bertotti G 1998 *Hysteresis in Magnetism* (New York: Academic)
[30] Song T and Roshko R M 2000 *Physica* B **275** 24
[31] Papvassiliou G, Fardis M, Belesi M, Maris T G, Kallias G, Pissos M, Niarchos D, Dimitropoulos C and Dolinski J 2000 *Phys. Rev. Lett.* **84** 761